

1 **Running head: high resolution cavitation- and frost-fatigue**

2

3

4

5 **Corresponding author:**

6 Melvin T. Tyree

7 College of Forestry, Northwest A&F University, Yangling, Shaanxi 712100, China

8 E-mail: mel.tyree@cantab.net

9 Telephone: +86 029 87080363

10

11

12

13 **Research area:**

14 Ecophysiology and Sustainability

15

16 **Investigations concerning cavitation- and frost-fatigue in clonal *Populus* 84K using ‘high
17 resolution’ cavitron measurements¹**

18

19 Feng Feng, Fei Ding, Melvin T. Tyree*

20

21 College of Forestry, Northwest A&F University, Yangling, Shaanxi 712100, China

22

23 *Author for correspondence mel.tyree@cantab.net

24

25

26

27

28 **Summary:**

29 Frost and drought induced 'fatigue' in *Populus* stems, which damaged vessels making them more
30 vulnerable to embolism in future; evidence supports a common mechanism causing both types of
31 fatigue.

32

33

34 **Footnotes**

35 ¹ This study was supported by the grants of “thousand talent program” to M.T.T.

36 * Corresponding author; email mel.tyree@cantab.net

37

38 **Abstract**

39 Both drought and freezing-thawing of stems induce a loss of hydraulic conductivity (PLC, percent
40 loss of conductivity) in woody plants. Drought induced PLC is often accompanied by physical
41 damage to pit membranes causing a shift in vulnerability curves (cavitation-fatigue). Hence if
42 cavitated stems are flushed to remove embolisms, the next vulnerability curve is different (shifted
43 to lower tensions). The *Populus* clone (84K *Populus alba*×*Populus glandulosa*) has small vessels
44 that should be immune from frost-induced PLC, but results demonstrated that freezing-thawing in
45 combination with tension synergistically increased PLC. Christensen-Dalsgaard & Tyree were the
46 first to define ‘frost-fatigue’ which is similar to cavitation-fatigue but induced by freezing. Frost-
47 fatigue caused a transition from a single- to a dual-Weibull curve but drought-fatigued stems had
48 single-Weibull curves shifted to lower tensions. Studying the combined impact of tension plus
49 freezing on fatigue provided evidence that the mechanism of frost-fatigue may be due to extra
50 water tension induced by freezing or thawing while spinning stems in a centrifuge rather than
51 direct ice-damage. A hypothesis is advanced that tension is enhanced as ice crystals grow or melt
52 during the freeze or thaw event, respectively, causing a nearly identical fatigue event as induced
53 by drought.

54

55

56 **INTRODUCTION**

57 Water transport in xylem conduits of trees occurs while water is under tension (= negative
58 pressure) (Tyree and Zimmermann, 2002). The xylem water-transport system is vulnerable to
59 cavitation and embolism, because tensile water is meta-stable so if a gas bubble appears in a
60 conduit it will rapidly expand to fill the conduit whenever the fluid tension is ≥ 0.1 MPa, where a
61 tension of 0.1 MPa is equivalent to vacuum-pressure. A cavitation event occurs whenever a tensile
62 water-column breaks which results in a water-vapor-filled void. Because of Henry's law of gas
63 solubility in water, this vapor-void will eventually equilibrate with air at atmospheric pressure at
64 which point the conduit is fully embolized (Tyree and Zimmermann, 2002). Embolism has been
65 identified as a limiting factor of primary production (Hubbard et al., 2001). As a result, tree
66 growth and fitness are probably negatively impacted temporarily or seriously limited permanently
67 if embolism is extensive (Christensen-Dalsgaard and Tyree, 2013).

68 The two main factors causing cavitation and embolism are drought and frost (Mayr et al.,
69 2003; Christensen-Dalsgaard and Tyree, 2013). Drought-induced cavitation is caused by the high
70 xylem tension attributed to water stress. The high tension in the sap forces air bubbles into
71 functional conduits from neighboring embolized ones through shared pit membranes (Jarbeau et
72 al., 1995; Sperry et al., 1996; Hacke et al., 2001; Stiller and Sperry, 2002; Christman et al., 2012)
73 according to "air seeding" mechanism (Sperry and Tyree, 1988; Cochard et al., 1992). Hence, the
74 continuity of water flow is disrupted due to cavitation. Frost-induced cavitation, on the other hand,
75 occurs when dissolved gases in the sap freeze out and create bubbles during ice formation because
76 air is not soluble in ice (Mayr et al., 2003; Christensen-Dalsgaard and Tyree, 2013, 2014) but
77 remains entrapped between ice crystals. Once the sap melts and tension is re-generated, the
78 entrapped bubbles may expand to embolize the conduits instead of dissolving (Pittermann and
79 Sperry, 2006). Current thinking is that freezing-induced embolism occurs when the tension
80 exceeds a critical value determined by the surface tension of the bubbles, which mainly depends
81 on the xylem water potential and the bubble radius (Yang and Tyree, 1992; Tyree et al., 1994;
82 Hacke and Sperry, 2001). Larger bubbles may form in conduits with a larger diameter, so species
83 with larger conduits are more vulnerable to frost-induced embolism (Langan et al., 1997; Davis et
84 al., 1999; Pittermann and Sperry, 2006). Furthermore, enhanced loss of hydraulic conductivity of
85 trees may occur when stems are subjected to a combination of frost-drought causing low xylem
86 water potential (Mayr et al., 2003; Willson and Jackson, 2006) and repeated freeze-thaw cycles
87 (Sperry and Sullivan, 1992; Cox and Zhu, 2003; Mayr et al., 2003). However, even trees with
88 small conduits are found to suffer severe embolism in winter (Sperry et al., 1988; Ameglio et al.,
89 2002) due mostly to freeze-drying of stems.

90 Resilient species are those which suffer no significantly different cavitation resistance before
91 and after a cavitation-refilling cycle (Hacke et al., 2001; Christensen-Dalsgaard and Tyree, 2013).
92 In contrast, species that are weakened by cavitation or frost are said to suffer cavitation-fatigue or
93 frost-fatigue. Cavitation and frost-fatigue is quantified by how much the vulnerability curve is
94 shifted before versus after a fatigue-inducing event, and it is typically reported as a shift in P_{50} .
95 The P_{50} is either the pressure (negative value) or tension (positive value) that produces 50 % loss
96 of hydraulic conductivity (K_h). In the rest of this paper we will use T_{50} to indicate the tension at
97 50 % loss of conductivity or T_x to indicate the tension that induces x % loss of conductivity.
98 Vulnerability curves (VCs) are usually measured by a centrifuge technique (Alder et al., 1997;
99 Cochard et al., 2005), but most people measure just 5 or 6 points to determine a VC. “High
100 resolution” VC curves with 9 to 27 points per curve can be collected quickly using the Cochard
101 rotor. Recent studies have successfully used high resolution VC to characterize the detailed shape
102 of VCs revealing dual-Weibull curves, e.g., r- and s- shaped or dual s-shaped curves (Cai et al.,
103 2014; Wang et al., 2014a), because a complex shape to a VC cannot be identified with just a few
104 points. Furthermore, we used a centrifuge to induce tension while simultaneously freezing in
105 order to study the combined impact of tension and freezing-thawing on frost-fatigue and freeze-
106 thaw-induced embolism.

107 In this paper, we intend to investigate whether drought and freeze-thaw cycles could have an
108 effect on the cavitation resistance in terminal shoots from adult trees of 84K poplar (*Populus alba*
109 \times *Populus glandulosa*), with high resolution analysis of VCs and artificial freeze-thaw simulation
110 technique. *Populus* are known to be water-demanding, drought-sensitive species with T_{50} ranging
111 from 1.07 to 2.5 MPa (Fichot et al., 2014) and vulnerable to winter damage (Feng et al., 2010).
112 Amongst poplars, 84K poplar is known by foresters to be relatively resistant to water stress, low
113 temperature, diseases and insects (Zhou et al., 2007). As the main afforestation species in
114 Shaanxi, Gansu and Qinghai Province, 84K is of great ecological importance.

115

116 **RESULTS**

117 **Cavitation-fatigue**

118 Vulnerability curves of 84K stems were measured 4 times; the first VC was measured in flushed,
119 native material and the other 3 VCs were obtained on the same stem segments after exposure to 3
120 cycles of flushing with 0.1 M KCl and 0.01 M CaCl₂ solutions followed by VC measurements.
121 All VCs were s-shaped and fit Weibull curves with an average route mean square error (RMS_{error})
122 of 2.31 %; see Fig. S1A for typical curves. The recovery of K_h after each flush cycle averaged
123 about 99.48 % for all experiments (Table I). The mean values \pm SE of tension (T_x) at 10 %
124 increments of PLC are shown in Table II together with results of a significance test between KCl

125 and CaCl₂ treatments. There was no significant difference between T_x values for KCl and CaCl₂
126 perfusions except between the 2nd and 3rd VC where CaCl₂ perfusion made the stems significantly
127 more vulnerable from $x = 10$ to 50 PLC.

128 The shift of vulnerability curves to the left in Fig. 1 indicated a loss of cavitation resistance
129 (cavitation-fatigue), but a shift to the right indicated a gain of cavitation resistance (recovery from
130 cavitation-fatigue). The significance of the shift in VCs was calculated two ways: shifts of mean
131 VCs and shift between stems (see Eq. 3 in Methods). The significance tests based on shifts of
132 means is shown in Table III. There were significant difference between the 1st versus 2nd, 1st
133 versus 3rd, and the 1st versus 4th VC for both KCl and CaCl₂ flushed stems and between the 2nd and
134 4th VCs for KCl flushed stems based on the means in Table II.

135 The significance test for shifts in the mean values of T_x were confounded by the population
136 variability of VCs between individual stems. A stronger test of the shift in T_x values is obtained by
137 using Eq. 3B to compute the means shift of all individual branches and testing if the shift is
138 significantly different from zero. The shifts can be computed as absolute cavitation-fatigue shifts
139 (aCF_x) or relative cavitation-fatigue shifts (rCF_x) as defined in Eq. 3 and these are shown as plots
140 in Fig. 2 and 3. Fig. 2 and 3 demonstrated that there was a positive increase in cavitation-fatigue
141 (positive aCF_x or rCF_x) between the 1st and 2nd VC. But there were small but significant
142 improvements (negative aCF_x or rCF_x) for most other cycles. Negative values of aCF_x or rCF_x
143 indicate the resistance to cavitation improved. Stems flushed by KCl solutions recovered more
144 than stems flushed with CaCl₂ solutions (Fig. 2&3).

145 **Frost-fatigue and frost-induced PLC**

146 The vulnerability curves of 84K poplar were sigmoid curves in all experiments even after
147 cavitation-fatigue had occurred (Fig. 1 and S1A). In contrast, our freeze-thaw treatments caused
148 significant change in the shape of the VCs measured after flushing. They changed from single to
149 dual s-shaped Weibull curves (Fig. 4 and S1B, Eq. 2B). Freeze-thaw cycles were conducted on
150 flushed stems at 4 different tensions 0.088, 0.5, 1.0 and 1.5 MPa while the stems were spinning in
151 a cavitron, and the mean flushed conductivity after the freeze-thaw event was ≥ 95 % of the
152 original (Table I). The highest two tensions were enough to cause some cavitation-fatigue in the
153 absence of freezing but there was a synergy between the freeze-thaw event and cavitation-fatigue
154 causing a higher loss of maximum conductivity (Fig. 5) than expected from cavitation-fatigue
155 alone. At the lowest three tensions the frost-fatigued curves were not significantly different and
156 involved a shift in the 10 to 15 % of most vulnerable vessels (Fig. 4). However, a freeze-thaw
157 cycle at tension = 1.5 MPa caused a significant increase in frost-fatigue.

158 The mean vessel diameter of 84K poplar was 28.70 ± 0.11 μm ($N = 4307$) and hence should
159 not be big enough to induce loss of conductivity during a freeze-thaw event (Hacke and Sperry,

160 2001) and this fact is confirmed in the near-zero tension value shown in Fig. 5; nevertheless frost-
161 fatigue occurred even at the lowest tension (Fig. 4). However increased tension caused a reduction
162 in maximum K_h (Fig. 5) wherein the loss of K_h exceeded that due to tension-induced cavitation
163 without freezing. This suggests that the freeze-thaw event caused an increase in tension (double
164 arrows in Fig. 5) during either the freezing or during thawing or both as explained in the
165 Discussion.

166 Frost-fatigue VCs looked very different from cavitation-fatigue VCs, because the former
167 transformed an s-shaped curve into a dual s-shaped curve whereas cavitation-fatigue shifted the
168 entire s-shaped curve to the left in Fig. 1 but it remained a simple s-curve. We postulated that
169 frost-fatigue might damage only the most vulnerable vessels, hence the nature of the damage
170 might be duplicated by cavitation-fatigue in only the lower half of the VC. To test this notion we
171 measured vulnerability curves of stems only to the 50 PLC value (Fig. 6, solid line), flushed the
172 stem then measured the VC again (Fig. 6, dashed curve). This procedure produced a dual Weibull
173 strikingly similar to our frost-fatigue curve (Fig. 4, dotted line).

174 **Field observations of frost-fatigue**

175 Vulnerability curves measured in four consecutive phenological phases were plotted in Fig. 7A.
176 The VCs were not significantly different from each other no matter how many freeze-thaw cycles
177 occurred during the winter (Table IV). The frequency of frost events in the winter of this study
178 can be deduced from the maximum and minimum temperatures shown in Fig. 7B, but the stems
179 might not have frozen every time the air temperature fell below 0 °C because of super-cooling.
180 However, once leaves were fully expanded values of T_{60} to T_{90} declined perhaps because of
181 growth of new vessels in spring. The frost-fatigue in early winter suggested that some of the early
182 winter freezing events were enough to cause some frost-fatigue that persisted into the spring.
183 Comparison of Fig. 7A to Fig. 4 through 5 suggests that the first natural freezing events in trees
184 might have been accompanied by an enhancement of xylem tensions of ≥ 0.5 MPa at the time of
185 the freeze-thaw events. Frost-fatigue hydraulically damaged about 16 % of the most vulnerable
186 vessels (Fig. 7A). These freeze-thaw events caused no significant shift in the T_{50} (see Table IV
187 and II), hence the events reported in this paper would not have been observed in previous studies
188 that reported only the impact of frost damage on T_{50} (Christensen-Dalsgaard and Tyree, 2013).
189 High resolution vulnerability curves are needed to document the cause of dual-s Weibull curves.
190 At the beginning of our research on 84K poplar, dual-s Weibull curves were observed in June and
191 July. By August the 84K poplar shoots grew enough for cavitron sized stem segments (0.274 m
192 long by 6 mm diameter) to include only current year shoots. Hence, when cavitation-fatigue
193 experiments began in August only s-shaped curves were observed (see Fig. 1). When the trees

194 flushed new leaves after winter, the vulnerability curves were still dual Weibull similar to those
195 measured in the winter.

196

197 **DISCUSSION**

198 The present study revealed two different fatigue responses in 84K poplar: a strong drought-
199 induced cavitation-fatigue and a weaker frost-induced fatigue. These will be discussed separately
200 below.

201 **Cavitation-fatigue: relative (rCF_x) and absolute (aCF_x)**

202 Many prior studies have described cavitation fatigue, see Hacke et al. (2001) and papers cited
203 therein. The unique findings of our study were: (1) That repeated cycles of cavitation and flushing
204 do not cause additional damage, i.e., repeated cycles of cavitation and flushing did not increase
205 the magnitude of fatigue (Fig. 1) rather our data showed significant partial recovery (Figs. 2 and
206 3). (2) That high resolution measurements of VCs revealed pattern of cavitation-fatigue in which
207 the rCF_x was a linear function of the tension (T_x) causing the fatigue (Fig. 2A and 3A) wherein the
208 most vulnerable vessels exhibit the most relative cavitation-fatigue. (3) That when minor recovery
209 from cavitation-fatigue occurred after three cycles of cavitation and flushing, the biggest recovery
210 occurred among the most vulnerable vessels. (4) That repeated cycles of flushing and cavitation
211 showed that CaCl_2 -flushed stems exhibited poorer recovery than KCl-flushed stems (see Fig. 2
212 and 3).

213 With regard to the last finding, we compared stems flushed with CaCl_2 versus KCl to
214 investigate the possible role of Ca^{2+} in stabilizing cell walls and pit membranes (Cosgrove, 1997;
215 van Ieperen and van Gelder, 2006). Cell walls are weak ion exchange resins containing mostly
216 polyuronic acids that normally favor the accumulation of Ca^{2+} at the weak acid exchange sites.
217 Repeated flushing with concentrated KCl would gradually eliminate nearly all Ca absorbed to the
218 exchange sites. Ca^{2+} might serve as a bridge between weak acid polymers that might add to the
219 stability of pit-membrane pores that seed cavitation. Our results conclusively show that washing
220 out Ca^{2+} by flushing with 0.1 M K^+ enhanced rather than weakened cavitation resistance from
221 which we might conclude that putative pit-membrane pores actually shrunk. In contrast, flushing
222 with Ca^{2+} made no difference compared to K^+ and may actually retard recovery from cavitation-
223 fatigue.

224 Trends of rCF_x versus T_x had slopes significantly different from zero. In other species of
225 *Populus* the vulnerability to cavitation (measured by the b constant in the Weibull function) was
226 linearly related with vessel diameter (Cai and Tyree, 2010). Hence it can be hypothesized that the
227 larger vessels have more relative cavitation-fatigue (rCF_x). More research is needed to confirm
228 this relationship. Values of rCF_x in other species are also worth documenting in the future.

229 In our study ‘drought’ was induced artificially in a centrifuge but it is generally assumed that
230 soil-based drought events will have the same impact on cavitation-fatigue, although there are few
231 examples proving that assumption with the notable exception of the well-documented case of
232 sunflower (Stiller and Sperry, 2002). In the case of sunflower, potted plants were dehydrated by
233 withholding water and the stem recovered from drought induced cavitation-fatigue within 4 days
234 of re-watering, whereas the excised stems cavitating in a centrifuge showed weak or no recovery.
235 Our study on 84K poplar also showed small but significant recovery from cavitation-fatigue.
236 More comparisons between whole plants and excised shoots need to be done to understand the
237 mechanism of recovery in whole plants. In a survey study of 7 species, Hacke et al. (2001) found
238 that three species were ‘resilient’ and four species were not resilient. Among the four species in
239 (Hacke et al., 2001) two were *Populus sp.* that exhibited cavitation-fatigue in agreement with our
240 84K-clone *Populus*. In contrast, Christensen-Dalsgaard and Tyree (2013) have reported the
241 Walker-clone *Populus* to be resilient in terms of T_{50} .

242 **Absolute Frost-fatigue (aFF_x) and Frost-Induced PLC**

243 In contrast to cavitation-fatigue in which the pre- and post-fatigued stems were both s-shaped,
244 frost-fatigue changed the VC from an s-shape to a dual s-shape. Most previous studies of frost-
245 fatigue (Hacke and Sperry, 2001) have focused on increased PLC after a freeze-thaw event and
246 frost-fatigue was measured as a shift of 4 to 5 point VCs of unfrozen versus frozen samples.
247 Christensen-Dalsgaard and Tyree (2014) focused on shifts of T_{25} , T_{50} and T_{90} from VCs with 6 to 7
248 points. Our study is unique in quantifying high resolution curves with > 20 points depending on
249 the complexity of the curve. High resolution curves are needed to accurately resolve complex
250 curve shapes.

251 From previous studies we would predict that 84K poplar would exhibit no PLC or frost-
252 fatigue following a freeze-thaw cycle because vessel diameter of 84K poplar (28 μm) was below
253 the critical diameter of 30 μm (Davis et al., 1999). Species with vessel-diameters 40 μm are
254 typically 100 % embolized after a freeze-thaw event whereas species with vessels between 30 and
255 40 μm diameter are intermediate (Davis et al., 1999). Our results demonstrated that tension in
256 combination with a freeze-thaw event caused more PLC than tension alone (see Fig. 5). Our study
257 is the first to demonstrate that species with vessels < 30 μm diameter are impacted when frozen
258 under tension, which caused increased PLC and frost-fatigue. It is not clear whether frost-induced
259 embolism is always accompanied by frost-fatigue nor do we fully understand the mechanism of
260 damage to pit membranes making them more vulnerable to cavitation after a freeze-thaw event.

261 Our results were consistent with the notion that a freeze-thaw event increased the centrifuge-
262 induced “background” tension present in the stem segment during the experiment. Hence more
263 research is justified to test the hypothesis that cavitation-fatigue and frost-fatigue might both be

264 manifestations of cavitation-fatigue. The idea that a common mechanism existed between frost-
265 and cavitation-fatigue was confirmed by the cavitation-fatigue experiment in which the first VC
266 was taken only to 50 % PLC, because when these stems were flushed the cavitation-fatigue that
267 resulted was strikingly similar to the frost-fatigue VC (compare Figs. 6 to 4).

268 Comparing the results in Fig. 5 (dashed line minus solid line) one can conclude that the
269 freeze-thaw cycle increased the tension by about 0.5 to 0.8 MPa (double headed arrows in Fig. 5).
270 Since water expands to form ice as it freezes and contracts as it thaws one might presume the
271 frost-fatigue occurred during the thaw. But this simple notion might be wrong, because when *Acer*
272 and *Juglans* stems freeze the tension often occurred during the freeze and positive pressure
273 occurred during the thaw. Readers should consult previous work on *Acer* for the detailed
274 explanation for this notable behavior (Tyree, 1983; Johnson et al., 1987; Cirelli et al., 2008).
275 Briefly, however, the development of tension is due to water migration into air-filled wood fiber
276 cells to form ice (O'malley and Milburn, 1983; Milburn and O'malley, 1984) during the freeze
277 event. The ice formation in the Milburn-O'Malley model is by vapor distillation from water in
278 vessels to ice-crystals growing in air-filled spaces and the distillation process will induce tension
279 in the liquid water. Our suggested interpretation of Fig. 5 is as follows: In flushed stems all wood
280 fiber cells are filled with water so freezing induces no extra tension hence there can be no freezing
281 induced PLC. But if the stems are put under tension before freezing then air-spaces are created in
282 some fiber cells where ice can form causing freezing-induced tension by the Milburn-O'Malley
283 model (Tyree 1983; Milburn and O'Malley 1984); the enhanced tension would then induce
284 cavitation before the vessels are totally frozen. However, the parsimonious explanation is that
285 bubbles entrapped in ice expand during the thaw while ice melts under tension. We reject the
286 parsimonious interpretation because a tension of 0.5 MPa should be enough to induce 100 %
287 embolism in all vessels because all vessels have air entrapped in ice. In contrast the Milburn-
288 O'Malley model predicts that tension will increase as the amount of air space for ice formation
289 increases and the volume of air-filled fibers might increase with tension. Future research may
290 resolve these conflicting ideas.

291 An alternative explanation is that ice-crystal formation somehow damages pit membranes
292 (Christensen-Dalsgaard and Tyree, 2014). For this to occur ice crystals have to grow faster on one
293 side of pit membrane than the other. This is highly likely to occur if one side has water that can
294 freeze but the other side has air, because as water expands 10 % to form ice the pit membrane
295 could be pushed towards the embolized side causing tensile failure to the membrane. In contrast,
296 if water and ice are present on both sides of the pit membrane the pressure of ice might oppose
297 each other equally resulting in no damage. This idea about 'one-sided' ice growth cannot be tested

298 in 84K poplar, because embolizing 50 % of the vessels induced about the same amount of fatigue
299 measured as a shift in vulnerability curve at the lower PLC-values as frost-fatigue.

300 Comparing Figs 1 and 6 reveals a shift of aCF_x (at $x = 10$ PLC) of about 1 MPa and this shift
301 is the same as the frost-fatigue shift (aFF_x) at 10 PLC (Figs. 4 and 7). It could be argued that ice-
302 induced damage to pit-membranes ought to be quite different from cavitation damage. During a
303 cavitation event only one pore out of millions of pores connecting adjacent vessels needs to be
304 plastically deformed to make a larger hole which makes the vessels more prone to cavitation in
305 subsequent VCs (Fig. 1). Based on surface tension arguments (Tyree and Zimmermann, 2002), we
306 can say that the diameter (D) of a pit membrane pore that induces cavitation should be $= \cos(\theta)$
307 $4\gamma/\Delta P$, where ΔP is the pressure difference inducing cavitation across the pore and θ is the contact
308 angle of the air/water interface at the pore surface and γ is the surface tension of the solution at the
309 pit pore. Frost- or cavitation-fatigue (aFF_x or aCF_x , respectively) equals the shift in ΔP to ΔP_f , i.e.,
310 from a normal to fatigued pressure difference inducing cavitation. Hence $D_f = D \Delta P/\Delta P_f$. The
311 shift of aCF_x at 10 PLC is $\Delta P = 1.5$ to $\Delta P_f = 0.5$ MPa from which it follows that the most fatigued
312 pore in the pit membrane is 3 times larger than the native pore (because $\Delta P/\Delta P_f = 3$). The
313 magnitude of $aCF_x = aFF_x$ in our study (at $x = 10$ PLC), which is a remarkable coincidence. One
314 might argue that if growth of ice-crystals is poking holes in pit membranes, the holes ought to
315 occur in thousands of membrane connecting adjacent vessels and it seems unlikely that the shift
316 aFF_x and aCF_x would be nearly identical. More experimental work might provide useful data to
317 resolve the above speculations.

318 We think much more can be learned about cavitation- and frost-fatigue through high
319 resolution measurement of vulnerability curves in a Cochard cavitron. At the time this study was
320 completed we could achieve fits to single or dual Weibull curves with RMS_{error} of about 2 %. The
321 RMS_{error} was primarily due to the error in estimation of K_h and K_{max} because $PLC = 100(1 -$
322 $K_h/K_{max})$. Subsequent to the completion of this study we were able to increase the precision of
323 measurements of K_h and K_{max} by a factor of 5 (Wang et al 2014b). The increase of precision was
324 achieved by using a regression method to estimate hydraulic conductivity values and by using a
325 centrifuge that can control temperature of the stem to ± 0.04 °C. Temperature control is important
326 because K_h is inversely proportional to $1/\text{viscosity}$ of water and the viscosity changes about 2.4 %
327 °C⁻¹. By using high resolution measurement (more points) and high precision measurements (more
328 accurate K_h), future studies on cavitation- and frost-fatigue may reveal more about the
329 mechanisms of damage and about the linkage, if any, between the two types of fatigue.

330

331

332 MATERIALS AND METHODS

333 Plant material

334 The study was carried out on the clonal *Populus* 84K (*Populus alba*×*Populus glandulosa*)
335 growing near Northwest A&F University, Yangling, Shaanxi, China (34°15'N 108°4'E, Elev. 457
336 m). The sampling was conducted at intervals from August to April over a fall-winter-spring
337 season in 2013-2014. All measurements were done on shoots that were not significantly water
338 stressed before collection because no evidence of cavitation-fatigue was observed in the first VC
339 after flush. Shoots 90- to 120- cm length were excised, because preliminary air-injection
340 experiments indicated that maximum vessel length was < 50 cm and mean about 6 cm, hence the
341 vessels are short enough relative to cavitron sample length to avoid 'open-vessel' artifacts
342 reported by Wang et al. (2014a). The branches were enclosed in humidified black plastic bags
343 after spraying leaves with water. Then they were transferred to the laboratory within 15 min and
344 submerged in water for at least 30 min to release tension. While submerged, a 27.4-cm-long
345 segment was cut from each branch using fresh razor blades. Leaves were removed when present.
346 These segments were exposed either to four consecutive cycles of cavitation-refilling or to a
347 freeze-thaw cycle in combination with tensile-water, imposed by spinning stems in a centrifuge.
348 Additional experiments were done on the same species to compare lab results with field
349 conditions throughout the winter and spring.

350 A vulnerability curve (VC) defines the relationship between percentage loss of hydraulic
351 conductivity (PLC) and the tension (T), where T = minus the xylem pressure potential. We used
352 the whole vulnerability curves to quantify "fatigue" over 9 equally spaced points on the y-axis of
353 the VC (for simple s-shaped curves). The cavitron technique was used to measure vulnerability
354 curves. Both cavitation and frost-fatigue were measured in terms of the shift of the vulnerability
355 curve along the tension axis.

356 Flushing with particle 'free' water

357 Clean flushing water was essential to prevent plugging of pit membranes in the segments (27.4
358 cm long) because one objective was to carry out 4 repeated cycles of cavitation-refilling on the
359 same stem with two different solutions: 0.1 M KCl and 0.01 M CaCl₂. The clean water system
360 below could repeatedly restore maximum conductivity (K_{max}) to 99.4±0.6% of the first K_{max} .

361 An ultrapure water system, model GYJ1-10L-S (Huachuang Inc., Chongqing, China) was
362 used which, according to specifications, produces water with less than one particle per ml of >10
363 nm diameter. Before flushing, freshly filtered water was produced each morning and reagent
364 grade KCl or CaCl₂ was added, and stored in a stainless steel captive air tank (CAT) model 3400-
365 002 (SHURflo Inc., Cypress, CA). The rubber bag inside the captive air tank was about 1.5 mm
366 thick and comprised 90 % of the surface area in contact with the salt solution. The lid and outlet

367 tubing was stainless steel. Contrary to popular belief, stainless steel is not rust free; rust is easily
368 observable in the rubber bag but it does not adhere to the stainless steel surfaces. We recommend
369 cleaning the tank twice per week to eliminate plugging-rust-particles gradually formed in the CAT.
370 The SHURflo CAT was selected because it could be disassembled by removing 6 retaining bolts
371 on the lid allowing removal of the rubber bag and access to the stainless steel parts normally in
372 contact with the salt solutions. All plastic and rubber tubing of the apparatus was cleaned with
373 bleach to kill micro-organisms followed by flushing twice with purified water. Also, the solution
374 in the tank was left unpressurized when not in use because air slowly permeates across the rubber
375 bag. We observed that leaving the tank pressurized for 24 h made the water weakly effervescent
376 which could cause bubble formation in stem segments during a flush.

377 **Cavitron measurements**

378 The measurements on hydraulic conductivity (K_h) and vulnerability curves (VCs) were carried out
379 using a custom rotor designed by Cochard et al. (2005) based on the centrifuge technique (Alder
380 et al., 1997). Design details were described in detail in Cai and Tyree (2010).

381 Briefly, this technique makes it possible to measure the K_h while the stem segment is
382 spinning at any given tension. A 27.4 cm segment is placed in the rotor mounted on the centrifuge.
383 Both ends of the segment are placed in cuvettes filled with liquid (0.1 M KCl or 0.01 M CaCl₂)
384 that could be replenished while spinning. A pressure difference generated by the different liquid
385 levels of the cuvettes drives the liquid through the segment. Then the rate of movement of the
386 liquid in the stem could be measured directly by a continuous calculation of the volume change in
387 the cuvettes within a certain time interval.

388 Prior to measurements, the stems were flushed with 0.1 M KCl or 0.01 M CaCl₂ at 40 PSI
389 (276 kPa) for 30 min to eliminate any native embolism. The length of time required to ensure all
390 conduits were refilled by the flush was determined in preliminary experiments as outlined in the
391 section “refilling and repeated cavitation cycles”. The rotor was rotated initially at 1000 RPM
392 (0.088 MPa) without a stem segment and the thermostat set a few °C below ambient room
393 temperature in order to have improved temperature control during measurement. Once all
394 conduits were refilled, K_{max} was measured at 1000 RPM (0.088 MPa) in the cavitron after a
395 stabilization time of 15 min. The tension caused by 1000 RPM was too small to cause any
396 embolism. Subsequently a VC was obtained through stepwise increases in the spin rate of the
397 centrifuge, subjecting the solution in the conduits to increasingly negative xylem pressures
398 (tension = minus pressure). The K_h was collected after a 2 min stabilizing time at each 200 RPM
399 increase. The percentage loss of hydraulic conductivity (PLC), which was attributed to embolized
400 conduits, was computed from:

$$401 \quad PLC = 100(1 - K_h/K_{max}) \quad \text{Eq. 1}$$

402 The spin rate was increased until K_h was reduced to a point where the PLC ≥ 90 %.

403 Vulnerability curves with ≥ 9 points was deemed sufficient to characterize simple s-shaped
404 Weibull curves. But 16 to 27 points are necessary to characterize a dual-Weibull curve.
405 Vulnerability curves, plots of PLC versus tension (T), were fitted to a single Weibull curve Eq. 2A
406 or a dual Weibull curve Eq. 2B through CavAnal software written by M.T.Tyree (Cai et al., 2014):

$$407 \quad PLC/100 = 1 - \exp[-(T/B)^C] \quad \text{Eq. 2A}$$

$$408 \quad PLC/100 = \alpha(1 - \exp[-(T/B_1)^{C_1}]) + (1-\alpha)(1 - \exp[-(T/B_2)^{C_2}]) \quad \text{Eq. 2B}$$

409 where the constants were calculated by minimizing root mean square error (RMS_{error}).

410 **Computation of cavitation-fatigue**

411 Between any two cycles of cavitation and flushing of the same stem, cavitation-fatigue was
412 computed based on absolute shift of T_x (defined above, $x = 10, 20 \dots 90$ PLC) from $T_{x,i}$ to $T_{x,j}$,
413 where i, j were the i^{th} and j^{th} VC ($j > i$). So for absolute cavitation-fatigue (aCF_x) we computed
414 $aCF_x = (T_{x,i} - T_{x,j})$ and for relative cavitation-fatigue (rCF_x) we computed $rCF_x = (1 - T_{x,j}/T_{x,i})$. The
415 means and standard error (SE) of each fatigue value was computed for all the stems in two
416 different ways. The first was the difference of the means (Eq. 3A) of N values and the second was
417 the mean of the differences (Eq. 3B) for N values. The two value of $\overline{aCF_x}$ are identical but in the
418 test of significance in the former we are asking if the means are significantly different whereas in
419 the latter we are asking if the difference is significantly different from zero, which was
420 statistically more certain (see results) because the phenotypic difference between individual stems
421 is eliminated by computing the mean of the different rather than the difference of the mean.

$$\overline{aCF_x} = \frac{1}{N} \left(\sum_{k=1}^N T_{x,i} - \sum_{k=1}^N T_{x,j} \right) \quad \text{Eq. 3A}$$

$$\overline{aCF_x} = \frac{1}{N} \sum_{k=1}^N (T_{x,i} - T_{x,j}) \quad \text{Eq. 3B}$$

422 The mean relative cavitation-fatigue (rCF_x) was computed from

$$\overline{rCF_x} = \frac{1}{N} \left(\sum_{i=1}^N (1 - T_{x,j}/T_{x,i}) \right) \quad \text{Eq. 3C}$$

423 These computations allowed us to compute the fatigue shifts for up to 4 cycles of cavitation
424 and flushing. Positive values of aCF_x and rCF_x measured loss in cavitation resistance and negative
425 values were interpreted as an increase in cavitation resistance.

426 **Temperature calibration**

427 Temperature control during VC measurement is important because K_h changes 2.4% °C⁻¹ as stem
428 temperature changes because of the effect of temperature on the viscosity of water. The Beckman-
429 Coulter centrifuge has a temperature sensor and thermostatic temperature control, but the factory
430 sensor is mounted too near the refrigeration coils hence large temperature differences were often
431 observed between the factory sensor and the sensor we installed near the rotor. The temperature
432 gradient was explained by the heat generated by the spinning rotor-motor (Wang et al., 2014b). In
433 order to correct for temperature gradients, a custom temperature sensor based on a LM335 sensor
434 chip was installed near the rotor midway between the refrigerated wall and rotor. The temperature
435 of the thermostat had to be adjusted down in temperature in order to achieve constant temperature
436 in the rotor as rotor RPM increased. Experiments were done to test the adequacy of temperature
437 control of the stem to within ± 1 °C.

438 Additional experiments were done to ensure we could stabilize temperature of the stems
439 within reasonable limits. Hydraulic conductivity was measured at constant RPM while changing
440 the thermostat temperature setting, which caused a corresponding rapid change in stem
441 temperature as confirmed by changes in K_h . The air temperature was logged every 10 s by our
442 independent sensor while periodically measuring K_h at constant RPM. The stem K_h acts like a
443 *defacto* thermometer because K_h changes in proportion to 1/viscosity of water. Preliminary
444 experiments were performed to ‘calibrate’ running mean values of air temperature to the ‘stem’
445 thermometer. We found out that a 20 min running mean of air temperature correlated
446 satisfactorily with the change in K_h when air temperature was changing rapidly (Fig. 8). Even
447 when the thermostatic temperature was set to a constant value the instantaneous air temperature
448 changed ± 2 °C as the refrigeration system turned on and off, but the 20 min running mean
449 changed less (± 0.5 to 1 °C) when the refrigeration turned on and off more than once per 5 minutes.

450 **Re-filling and repeated cavitation cycles (How long is enough for flushing?)**

451 Preliminary experiments were done to determine the length of time required to refill the
452 embolized conduits flushed at 276 kPa (40 PSI). The original conductivity (K_n) of each branch
453 prior to flushing was measured at 1000 RPM (0.088 MPa) in the cavitron. The stem was then
454 subjected to alternating 5 min cycles of flushing and conductivity measurements until the
455 conductivity stabilized (did not change for three consecutive cycles of flushing). Following this,
456 the vulnerability curve of the stem was measured.

457 This cycle of flushing to K_{max} and measurement of a VC was repeated 4 times. Thirty min of
458 flushing was enough to achieve a stable K_h . On average K_h was returned to the same K_{max} as
459 measured by the ratio of 100 % $K_{flushed}/K_{max}$ to within $99.4 \pm 0.6\%$. If K_h failed to reach ≥ 93 %
460 following a cavitation/flush cycle then the data was thrown out.

461 **Freeze-thaw cycles**

462 The stems were directly flushed for 30 min at 276 kPa with 0.1 M KCl solution after collection.
463 Unlike methods from other studies (Ameglio et al., 2001; Willson and Jackson, 2006;
464 Christensen-Dalsgaard and Tyree, 2013), we froze and thawed the plant material at known
465 tensions in the stems while spinning in a cavitron. We chose tensions of 0.08, 0.5, 1.0 and 1.5
466 MPa to continue the frost-fatigue test. In experimentally simulated freeze-thaw cycles, the stems
467 were exposed to freezing approximately for 2 h at -5°C (Fig. 9, thick line) and simultaneously to
468 tensions (RPM) of 0.08 (1000), 0.5 (2400), 1.0 (3400) and 1.5 MPa (4100) respectively, following
469 K_{max} measurements at 1000 RPM. Then the stems were thawed to the room temperature at the
470 same tension. The conductivity after freeze-thaw treatment was measured. Subsequently, the same
471 stems were removed, flushed for 30 min and a new VC was measured.

472 **Partial versus full vulnerability curves comparison**

473 In order to illustrate the connection between cavitation and frost-fatigue in 84K poplar, two
474 different vulnerability curves were measured. The liquid used for flushing was 0.1 M KCl. The 1st
475 VC after flushing was stopped at 50 % embolism, then the stem was removed and flushed again
476 and then the VC was determined to > 95 % PLC.

477 **Field conditions**

478 Four phenological phases from fall to winter and into the next spring, including natural frost stage
479 after the first freezing events of winter, budding stage, leaf-flushing stage and mature-leaf stage
480 were selected for VCs measurements, in order to see if the trees growing outside showed a pattern
481 of frost-fatigue like that induced in cavitron experiments. In all of these four stages, stems were
482 used to measure VCs directly after flushing for 30 min with 0.1 M KCl solution at 276 kPa.

483 **Statistics**

484 All statistical analysis were done with the SPSS 18.0 statistics package for PC (SPSS Inc.,
485 Chicago, IL, USA) using the 0.05 significance level. Comparisons of more than two groups
486 between all means were made with one-way ANOVA and the Duncan test. Student's *t*-tests were
487 used to compare means between two groups or differences of means from zero when appropriate.

488

489 **SUPPLEMENTAL DATA**

490 Figure S1. Typical examples of “high resolution” VC curves with 9 to 27 points measured by
491 Cochard rotor.

492

493 **ACKNOWLEDGEMENTS**

494 We thank Ruihua Pan for conduits diameter measurements, Ruiqing Wang, Yujie Wang, Lingling
495 Zhang and Rongting Zhang for helpful assistance.

497 **LITERATURE CITED**

- 498 **Alder NN, Pockman WT, Sperry JS, Nuismer S** (1997) Use of centrifugal force in the study of
 499 xylem cavitation. *J Exp Bot* **48**: 665-674
- 500 **Ameglio T, Bodet C, Lacoite A, Cochard H** (2002) Winter embolism, mechanisms of xylem
 501 hydraulic conductivity recovery and springtime growth patterns in walnut and peach trees.
 502 *Tree Physiol* **22**: 1211-1220
- 503 **Ameglio T, Cochard H, Ewers FW** (2001) Stem diameter variations and cold hardiness in walnut
 504 trees. *J Exp Bot* **52**: 2135-2142
- 505 **Cai J, Li S, Zhang H, Zhang S, Tyree MT** (2014) Recalcitrant vulnerability curves: methods of
 506 analysis and the concept of fibre bridges for enhanced cavitation resistance. *Plant Cell Environ*
 507 **37**: 35-44
- 508 **Cai J, Tyree MT** (2010) The impact of vessel size on vulnerability curves: data and models for
 509 within-species variability in saplings of aspen, *Populus tremuloides* Michx. *Plant Cell Environ*
 510 **33**: 1059-1069
- 511 **Christensen-Dalsgaard KK, Tyree MT** (2013) Does freezing and dynamic flexing of frozen
 512 branches impact the cavitation resistance of *Malus domestica* and the *Populus* clone Walker?
 513 *Oecologia* **173**: 665-674
- 514 **Christensen-Dalsgaard KK, Tyree MT** (2014) Frost fatigue and spring recovery of xylem vessels in
 515 three diffuse-porous trees *in situ*. *Plant Cell Environ* **37**: 1074-1085
- 516 **Christman MA, Sperry JS, Smith DD** (2012) Rare pits, large vessels and extreme vulnerability to
 517 cavitation in a ring-porous tree species. *New Phytol* **193**: 713-720
- 518 **Cirelli D, Jagels R, Tyree MT** (2008) Toward an improved model of maple sap exudation: the
 519 location and role of osmotic barriers in sugar maple, butternut and white birch. *Tree Physiol*
 520 **28**: 1145-1155
- 521 **Cochard H, Cruziat P, Tyree MT** (1992) Use of positive pressures to establish vulnerability curves
 522 - further support for the air-seeding hypothesis and implications for pressure-volume analysis.
 523 *Plant Physiol* **100**: 205-209
- 524 **Cochard H, Damour G, Bodet C, Tharwat I, Poirier M, Ameglio T** (2005) Evaluation of a new
 525 centrifuge technique for rapid generation of xylem vulnerability curves. *Physiologia*
 526 *Plantarum* **124**: 410-418
- 527 **Cosgrove DJ** (1997) Relaxation in a high-stress environment: the molecular bases of extensible cell
 528 walls and cell enlargement. *The Plant Cell* **9**: 1031-1041
- 529 **Cox RM, Zhu XB** (2003) Effects of simulated thaw on xylem cavitation, residual embolism, spring
 530 dieback and shoot growth in yellow birch. *Tree Physiol* **23**: 615-624
- 531 **Davis SD, Sperry JS, Hacke UG** (1999) The relationship between xylem conduit diameter and
 532 cavitation caused by freezing. *American Journal of Botany* **86**: 1367-1372
- 533 **Feng LR, Song LZ, Lin XF** (2010) Research development of cold hardiness in *Populus* breeding.
 534 *Ecology Evolution and Systematics* **4**: 97-115
- 535 **Fichot R, Brignolas F, Cochard H, Ceulemans R** (2014) Vulnerability to Drought-Induced
 536 Cavitation in Poplars: Synthesis and Future Opportunities. *Plant Cell Environ*:
 537 10.1111/pce.12491
- 538 **Hacke UG, Sperry JS** (2001) Functional and ecological xylem anatomy. *Perspectives In Plant*
 539 *Ecology Evolution And Systematics* **4**: 97-115
- 540 **Hacke UG, Stiller V, Sperry JS, Pittermann J, McCulloh KA** (2001) Cavitation fatigue. Embolism
 541 and refilling cycles can weaken the cavitation resistance of xylem. *Plant Physiol* **125**: 779-786
- 542 **Hubbard RM, Ryan MG, Stiller V, Sperry JS** (2001) Stomatal conductance and photosynthesis
 543 vary linearly with plant hydraulic conductance in ponderosa pine. *Plant Cell And Environment*
 544 **24**: 113-121
- 545 **Jarbeau JA, Ewers FW, Davis SD** (1995) The mechanism of water-stress-induced embolism in two
 546 species of chaparral shrubs. *Plant Cell Environ* **18**: 189-196
- 547 **Johnson RW, Tyree MT, Dixon MA** (1987) A requirement for sucrose in xylem sap flow from
 548 dormant maple trees. *Plant Physiol* **84**: 495-500
- 549 **Langan SJ, Ewers FW, Davis SD** (1997) Xylem dysfunction caused by water stress and freezing in
 550 two species of co-occurring chaparral shrubs. *Plant Cell Environ* **20**: 425-437

- 551 **Mayr S, Gruber A, Bauer H** (2003) Repeated freeze-thaw cycles induce embolism in drought
552 stressed conifers (Norway spruce, stone pine). *Planta* **217**: 436-441
- 553 **Milburn JA, O'malley PER** (1984) Freeze-induced sap absorption in *Acer pseudoplatanus*: a
554 possible mechanism. *Canadian Journal of Botany* **62**: 2101-2106
- 555 **O'malley PER, Milburn JA** (1983) Freeze-induced fluctuations in xylem sap pressure in *Acer*
556 *pseudoplatanus*. *Canadian Journal of Botany* **61**: 3100-3106
- 557 **Pittermann J, Sperry JS** (2006) Analysis of freeze-thaw embolism in conifers. The interaction
558 between cavitation pressure and tracheid size. *Plant Physiol* **140**: 374-382
- 559 **Sperry JS, Donnelly JR, Tyree MT** (1988) Seasonal occurrence of xylem embolism in sugar maple
560 (*Acer Saccharum*). *Botanical Society of America* **75**: 1212-1218
- 561 **Sperry JS, Saliendra NZ, Pockman WT, Cochard H, Cruiziat P, Davis SD, Ewers FW, Tyree**
562 **MT** (1996) New evidence for large negative xylem pressures and their measurement by the
563 pressure chamber method. *Plant Cell Environ* **19**: 427-436
- 564 **Sperry JS, Sullivan JE** (1992) Xylem embolism in response to freeze-thaw cycles and water stress in
565 ring-porous, diffuse-porous, and conifer species. *Plant Physiol* **100**: 605-613
- 566 **Sperry JS, Tyree MT** (1988) Mechanism of water stress-induced xylem embolism. *Plant Physiol* **88**:
567 581-587
- 568 **Stiller V, Sperry JS** (2002) Cavitation fatigue and its reversal in sunflower (*Helianthus annuus* L.). *J*
569 *Exp Bot* **53**: 1155-1161
- 570 **Tyree MT** (1983) Maple sap uptake, exudation, and pressure changes correlated with freezing
571 exotherms and thawing endotherms. *Plant Physiol* **73**: 277-285
- 572 **Tyree MT, Davis SD, Cochard H** (1994) Biophysical perspectives of xylem evolution - is there a
573 tradeoff of hydraulic efficiency for vulnerability to dysfunction. *Iawa Journal* **15**: 335-360
- 574 **Tyree MT, Zimmermann MH** (2002) Xylem structure and the ascent of sap, Ed 2. Springer-Verlag,
575 Berlin, Germany
- 576 **van Ieperen W, van Gelder A** (2006) Ion-mediated flow changes suppressed by minimal calcium
577 presence in xylem sap in *Chrysanthemum* and *Prunus laurocerasus*. *J Exp Bot* **57**: 2743-2750
- 578 **Wang R, Zhang L, Zhang S, Cai J, Tyree MT** (2014a) Water relations of *Robinia pseudoacacia* L.:
579 do vessels cavitate and refill diurnally or are R-shaped curves invalid in *Robinia*? *Plant Cell*
580 *Environ* **37**: 2667-2678
- 581 **Wang YJ, Burlett R, Feng F, Tyree MT** (2014b) Improved precision of hydraulic conductance
582 measurements using a Cochard rotor in two different centrifuges. *Journal of Plant Hydraulics*
583 **1**: 0007e
- 584 **Willson CJ, Jackson RB** (2006) Xylem cavitation caused by drought and freezing stress in four co-
585 occurring *Juniperus* species. *Physiologia Plantarum* **127**: 374-382
- 586 **Yang S, Tyree MT** (1992) A theoretical-model of hydraulic conductivity recovery from embolism
587 with comparison to experimental-data on *Acer Saccharum*. *Plant Cell Environ* **15**: 633-643
- 588 **Zhou YX, Fu YQ, Fan JF, Liu YY, Gao JS, Wang J, Fu J, Li JA** (2007) Growth characteristics and
589 crossability of poplar 84K. *Journal of Northeast Forestry University* **35**: 11-12

590

591

592 Figure 1. Plotted are mean vulnerability curves measured for the same stem exposed to 4 cycles of
593 cavitation-refilling (flushing) and VCs measurements with 0.1 M KCl solution (A) and 0.01 M
594 CaCl₂ solution (B). The mean and SE (N = 7 for KCl values and N = 6 for CaCl₂ values) of all
595 curves were computed. See Table I for the % recovery of hydraulic conductivity after flushes.

596

597 Figure 2. This shows two quantitative measures of cavitation-fatigue for KCl flushed samples.
598 The fatigue values were calculated from the mean of the differences Eq. 3B (see methods), and is
599 considered a more powerful test of differences between VCs. A: Mean relative cavitation-fatigue
600 (rCF_x) versus x = the PLC at which rCF_x was evaluated. Solid squares compare 1st to 2nd VC, $y =$
601 $-0.3612x + 74.012$ ($R^2 = 0.9952, p = 2E-09$); solid triangles compare 2nd to 3rd VC, $y = 0.2335x -$
602 31.992 ($R^2 = 0.9444, p = 1E-05$); solid circles compare 3rd to 4th VC, $y = 0.1436x - 16.341$ ($R^2 =$
603 $0.95, p = 8E-06$); and solid diamonds compare 2nd to 4th VC, $y = 0.43x - 52.274$ ($R^2 = 0.9489, p$
604 $= 9E-06$). B: Mean change in absolute cavitation-fatigue (aCF_x) versus x = the PLC at which aCF_x
605 was evaluated. Hollow squares compare 1st to 2nd VC, $y = -7E-05x^2 + 0.0086x + 0.9352$ ($R^2 =$
606 $0.9758, p = 1E-5$), however, the individual points were not different from each other significantly
607 ($p = 0.334$); hollow triangles compare 2nd to 3rd VC, $y = -0.0006x - 0.1146$ ($R^2 = 0.7535, p$
608 $= 0.0024$); hollow circles compare 3rd to 4th VC, $y = 0.0004x - 0.099$ ($R^2 = 0.5669, p = 0.019$); and
609 hollow diamonds compare 2nd to 4th VC, $y = 3E-05x^2 - 0.0029x - 0.1636$ ($R^2 = 0.9877, p = 2E-6$).
610 Error bars are SE. Symbols marked without ‘*’ marks were not significantly different from zero.
611 The p -values in the linear regressions give the probability that the slope is zero.

612

613 Figure 3. This shows two quantitative measures of cavitation-fatigue for CaCl₂ flushed samples.
614 The fatigue values were calculated from the mean of the differences Eq. 3B (see methods), and is
615 considered a more powerful test of differences between VCs. A: Mean relative cavitation-fatigue
616 (rCF_x) versus x = the PLC at which rCF_x was evaluated. Solid squares compare 1st to 2nd VC, $y =$
617 $-0.3333x + 68.857$ ($R^2 = 0.9961, p = 1E-09$); solid triangles compare 2nd to 3rd VC, $y = -0.0018x +$
618 0.1707 ($R^2 = 0.9233, p = 4E-05$); and solid circles compare 3rd to 4th VC, $y = 0.3293x - 42.064$ (R^2
619 $= 0.9413, p = 1E-05$). B: Mean change in absolute cavitation-fatigue (aCF_x) versus x = the PLC at
620 which aCF_x was evaluated. Hollow squares compare 1st to 2nd VC, $y = -6E-05x^2 + 0.0078x +$
621 0.8899 ($R^2 = 0.9661, p = 4E-05$), however, the individuals were not different from each other
622 significantly ($p = 0.408$); hollow triangles compare 2nd to 3rd VC, $y = -0.0005x + 0.1225$ ($R^2 =$
623 $0.58, p = 0.017$); hollow circles compare 3rd to 4th VC, $y = -0.0009x - 0.1599$ ($R^2 = 0.8087, p =$
624 0.001). Error bars are SE. Symbols with no ‘*’ marks were not significantly different from zero.
625 The p -values in the linear regressions give the probability that the slope is zero.

626

627 Figure 4. Vulnerability curves measured in stems following a freeze-thaw cycle (f-t) at varying
628 tension. Frost induced embolism was removed by flushing before measuring the above VCs,
629 hence the double s-curves were caused by frost-fatigue. The mean of 6~8 VCs were measured on
630 flushed stems by the cavitron technique where each curve was fitted with a dual Weibull, then the
631 mean and SE of all 6~8 best-fit curves were computed.

632

633 Figure 5. The squares show the impact of freezing on changes of K_h expressed as % of K_{max} before
634 freezing. Error bars are \pm SE (N = 6 to 8). The y-axis can also be interpreted as 100% - the PLC
635 induced by freezing + the tension on the x-axis. The solid line is a Weibull equation fit of the
636 squares. The dashed line shows the mean impact of tension alone, without freezing, on %
637 maximum K_h ; these values were re-plotted from the 1st VC in Fig. 1A (100% - PLC induced by
638 tension alone). The double arrow can be interpreted as the amount of tension added by the
639 freezing or thawing of tissue.

640

641 Figure 6. Vulnerability curves measured before and after 50 % embolism induced in stems. The
642 mean and SE of all 6 best-fit curves before (solid curve) and after (dashed curve) 50% embolism
643 was induced by a tension of about 2.25 MPa; the stems were flushed between the first and second
644 curve. The dashed curve was fitted with a dual Weibull, which is the sum of two s-shaped Weibull
645 curves.

646

647 Figure 7. A: Vulnerability curves measured when stems were in four phenological phases, natural
648 frost stage, budding stage, leaf-flush stage and mature-leaf stage. VCs measurements in the
649 natural frost stage were based on N = 12 samples. VCs measurements in the budding stage and
650 leaf-flush stage were based on N = 6 samples respectively. The mature-leaf stage were based on N
651 = 7 samples. The mean of these VCs measured on flushed stems by the cavitron technique where
652 each curve was fitted with a dual Weibull, then the mean and SE were computed from the
653 individual Weibull curves. The dual Weibull fit is the sum of two Weibull curves, the first s-
654 shaped Weibull of each phenological phases are plotted to their theoretical plateaus for clarity and
655 the plateau values on the y-axis = α in Eq. 2B. B: Shows a plot of minimum and maximum air
656 temperatures recorded by a weather station 4 km of the location of the sampled trees.

657

658 Figure 8. A: This shows the tempo of change in air temperature and the 20 min running mean of
659 air temperature measured 2 cm from the rotor during the experiment shown in B. B: Shows the K_h
660 in stem versus the 20 min running mean of air temperature (RmTC20). The regression of K_h
661 versus RmTC20 was $y = 0.0648x + 1.8474$, $R^2 = 0.9826$, $p \leq 10^{-23}$, and the close correlation

662 means that the 20 min running mean air temperature was an acceptable predictor of stem
663 temperature. However the dependence of K_h on stem temperature was a less (lower slope) than
664 predicted from 1/viscosity of water in an ideal pipe (TheorStem), which had a regression of $y =$
665 $0.0774x + 1.8472$, $R^2 = 0.9994$, $p \leq 10^{-23}$.

666

667 Figure 9. This shows a typical plot of temperature versus time for a typical freeze-thaw cycle. Air
668 temperature (thin line) in the cavitron was collected every 10s. However, 20 min running mean of
669 air temperature (thick line) reflected more precisely the correct stem temperature (see Fig. 8). The
670 stems thawed more slowly than they froze because the centrifuge did not have active heating;
671 hence the stems and centrifuge was passively heated by the warm lab.

672

673 Figure S1. Typical examples of “high resolution” VC curves with 9 to 27 points measured by
674 Cochard rotor. A: Typical examples of VC curves with 9 to 13 points measured in cavitation-
675 fatigue experiments. B: Typical examples of VC curves with 24 to 25 points measured after
676 freeze-thaw treatment.

677

Table I. Percentage restoration of conductivity (K_{h_i}) after flushing followed by VCs measurement using 0.1 M KCl and 0.01 M CaCl₂ solution, respectively. Letter i represents the i^{th} flush followed by the i^{th} VC measurement ($i = 1, 2, 3, 4$). The data are based on means \pm SE of 7 samples (KCl) and 6 samples (CaCl₂). Also shown is percentage recovery of K_h after a freeze/thaw event in stems flushed with KCl at different freeze-thaw tensions (F-T Tension); shown are mean \pm SE of N = 6 to 8. $K_{f-t} = K_h$ recovered by flushing after the freeze-thaw event and $K_{max} = K_h$ of flushed stems before freezing.

Solution	K_{h_2}/K_{h_1}	K_{h_3}/K_{h_1}	K_{h_4}/K_{h_1}	
KCl	100.2 \pm 1.7%	100.2 \pm 0.9%	95.4 \pm 1.1%	
CaCl ₂	98.0 \pm 1.3%	103.1 \pm 1.9%	100.0 \pm 1.4%	
F-T Tension (MPa)	0.088	0.50	1.0	1.5
K_{f-t}/K_{max}	100.85 \pm 1.58%	98.68 \pm 2.01%	97.11 \pm 2.09%	95.40 \pm 1.50%

Table II. Statistical analysis of VCs measured in the same stem undergoing 4 cycles of cavitation-refilling and VCs measurements with 0.1 M KCl and 0.01 M CaCl₂ solutions respectively. Significance tests focus on the impact of salts (KCl vs CaCl₂) used for the flush. T_x represents the tension at which certain percentage loss of conductivity was caused (10, 20 ... 90 %). The values are means \pm SE of 7 samples using 0.1 M KCl solution and 6 samples using 0.01 M CaCl₂ solution. Significance levels (testing the impact of solution at any PLC): ‘*’ means $p < 0.05$.

PLC (%)	1 st VC		2 nd VC		3 rd VC		4 th VC		
	T_x (KCl)	T_x (CaCl ₂)	T_x (KCl)	T_x (CaCl ₂)	T_x (KCl)	T_x (CaCl ₂)	T_x (KCl)	T_x (CaCl ₂)	
10	1.38 \pm 0.1	1.41 \pm 0.1	0.38 \pm 0.0	0.46 \pm 0.0	0.48 \pm 0.0	0.35 \pm 0.0	*	0.56 \pm 0.0	0.50 \pm 0.0
20	1.64 \pm 0.1	1.66 \pm 0.1	0.54 \pm 0.0	0.63 \pm 0.0	0.67 \pm 0.0	0.52 \pm 0.0	*	0.75 \pm 0.0	0.69 \pm 0.0
30	1.82 \pm 0.1	1.84 \pm 0.0	0.68 \pm 0.0	0.77 \pm 0.0	0.81 \pm 0.0	0.66 \pm 0.0	*	0.90 \pm 0.0	0.86 \pm 0.0
40	1.98 \pm 0.0	2.00 \pm 0.0	0.81 \pm 0.0	0.90 \pm 0.1	0.95 \pm 0.0	0.79 \pm 0.0	*	1.04 \pm 0.0	1.00 \pm 0.0
50	2.12 \pm 0.0	2.14 \pm 0.0	0.93 \pm 0.0	1.03 \pm 0.1	1.08 \pm 0.0	0.92 \pm 0.0	*	1.17 \pm 0.0	1.13 \pm 0.0
60	2.27 \pm 0.0	2.28 \pm 0.0	1.07 \pm 0.1	1.16 \pm 0.1	1.22 \pm 0.0	1.06 \pm 0.0		1.31 \pm 0.0	1.28 \pm 0.0
70	2.42 \pm 0.0	2.43 \pm 0.0	1.22 \pm 0.1	1.31 \pm 0.1	1.38 \pm 0.0	1.21 \pm 0.0		1.45 \pm 0.0	1.44 \pm 0.1
80	2.59 \pm 0.0	2.60 \pm 0.0	1.40 \pm 0.1	1.49 \pm 0.1	1.56 \pm 0.0	1.41 \pm 0.1		1.63 \pm 0.0	1.63 \pm 0.1
90	2.83 \pm 0.0	2.82 \pm 0.0	1.67 \pm 0.1	1.74 \pm 0.1	1.82 \pm 0.1	1.68 \pm 0.1		1.87 \pm 0.0	1.91 \pm 0.1

Table III. Significance analysis results are shown for VCs quantified in Table II. The significance tests focused on the differences between VC curve numbers: 1, 2, 3, or 4 based on the means in Table II for VCs measurements with 0.1 M KCl solution (left) or 0.01 M CaCl₂ solution (right). T_x represents the tension at which certain percentage loss of conductivity was caused (10, 20 ... 90 %). Letters i and j indicate the i^{th} VC after the i^{th} flushing and the j^{th} VC after the j^{th} flushing, respectively. The significance analysis of VCs with KCl solution was based on $N = 7$ samples. The CaCl₂ solution VCs were based on $N = 6$ samples. Significance levels (testing the impact of solution at any PLC): ‘*’ means $p < 0.05$.

i^{th} VC vs j^{th} VC	T_x (KCl)									T_x (CaCl ₂)								
	10	20	30	40	50	60	70	80	90	10	20	30	40	50	60	70	80	90
1 st vs 2 nd	*	*	*	*	*	*	*	*	*	*	*	*	*	*	*	*	*	*
1 st vs 3 rd	*	*	*	*	*	*	*	*	*	*	*	*	*	*	*	*	*	*
1 st vs 4 th	*	*	*	*	*	*	*	*	*	*	*	*	*	*	*	*	*	*
2 nd vs 3 rd																		
2 nd vs 4 th		*	*	*	*	*	*											
3 rd vs 4 th																		

Table IV. Significance analysis of tensions at any given PLC in vulnerability curves of four phenological phases in stems collected from trees growing outdoors. T_x represents the tension at which certain percentage loss of conductivity was caused (10, 20 ... 90 %). Data are based on means \pm SE. The same small letters indicate the significant difference $p > 0.05$

T_x	Phenological Phase			
	Natural frost	budding	Leaf-flushing	Mature-leaf
T_{10}	0.84 \pm 0.12a	0.65 \pm 0.07a	1.06 \pm 0.26a	0.96 \pm 0.15a
T_{20}	1.47 \pm 0.14a	1.17 \pm 0.19a	1.52 \pm 0.23a	1.56 \pm 0.11a
T_{30}	1.80 \pm 0.11a	1.55 \pm 0.21a	1.87 \pm 0.12a	1.79 \pm 0.09a
T_{40}	2.05 \pm 0.08a	1.96 \pm 0.12a	2.07 \pm 0.07a	1.95 \pm 0.07a
T_{50}	2.23 \pm 0.07a	2.22 \pm 0.06a	2.23 \pm 0.05a	2.08 \pm 0.05a
T_{60}	2.39 \pm 0.06a	2.41 \pm 0.05a	2.36 \pm 0.05ab	2.20 \pm 0.05b
T_{70}	2.53 \pm 0.06a	2.59 \pm 0.04a	2.49 \pm 0.06a	2.31 \pm 0.04b
T_{80}	2.71 \pm 0.07a	2.77 \pm 0.03a	2.63 \pm 0.08a	2.44 \pm 0.05b
T_{90}	2.95 \pm 0.07a	3.01 \pm 0.05a	2.80 \pm 0.10ab	2.61 \pm 0.06b

— 1st VC - - 2nd VC - · - · - 3rd VC · · · · 4th VC

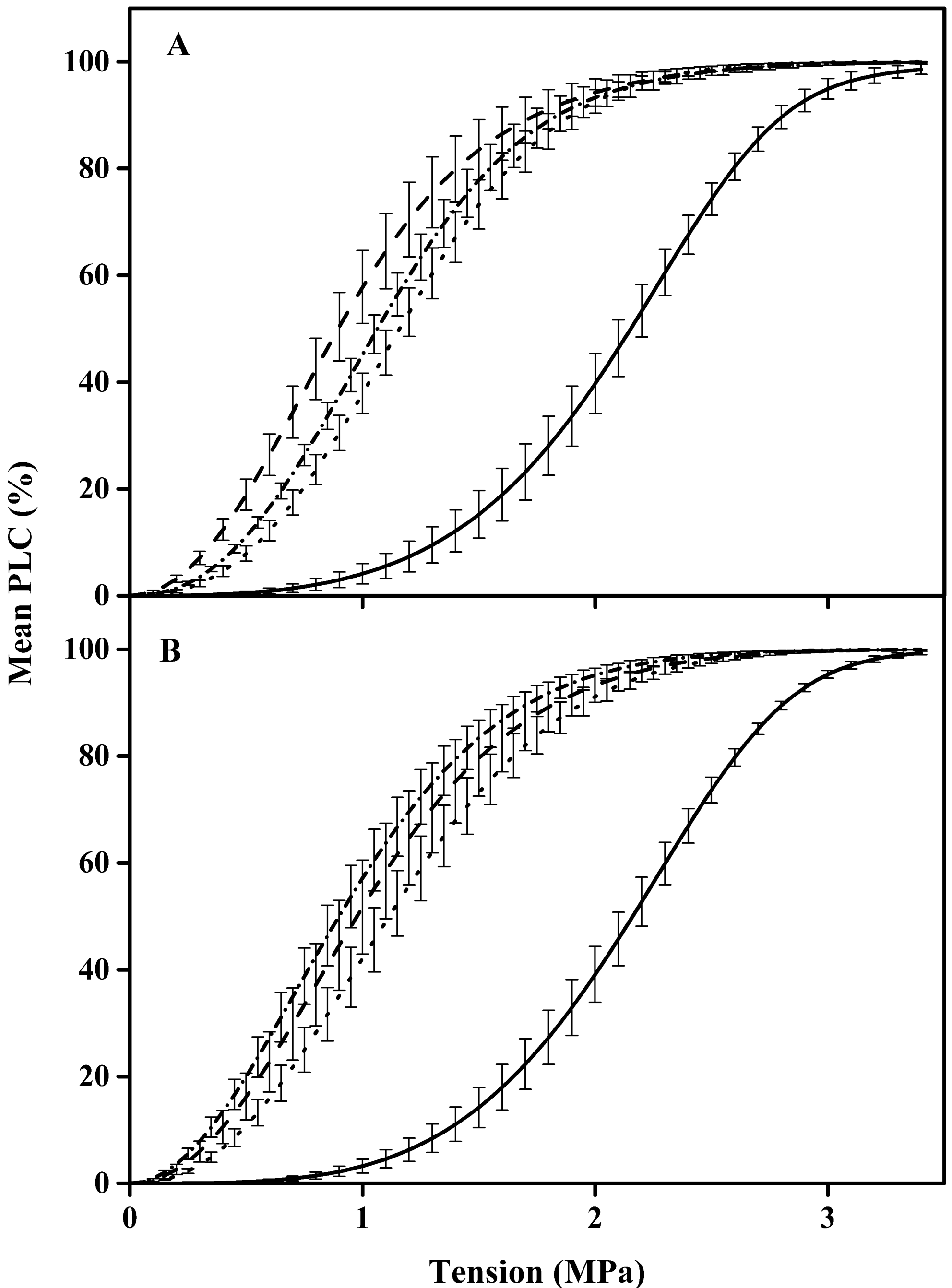


Figure 1. Plotted are mean vulnerability curves measured for the same stem exposed to 4 cycles of cavitation-refilling (flushing) and VCs measurements with 0.1 M KCl solution (A) and 0.01 M CaCl₂ solution (B). The mean and SE (N = 7 for KCl values and N = 6 for CaCl₂ values) of all curves were computed. See Table I for the % recovery of hydraulic conductivity after flushes.

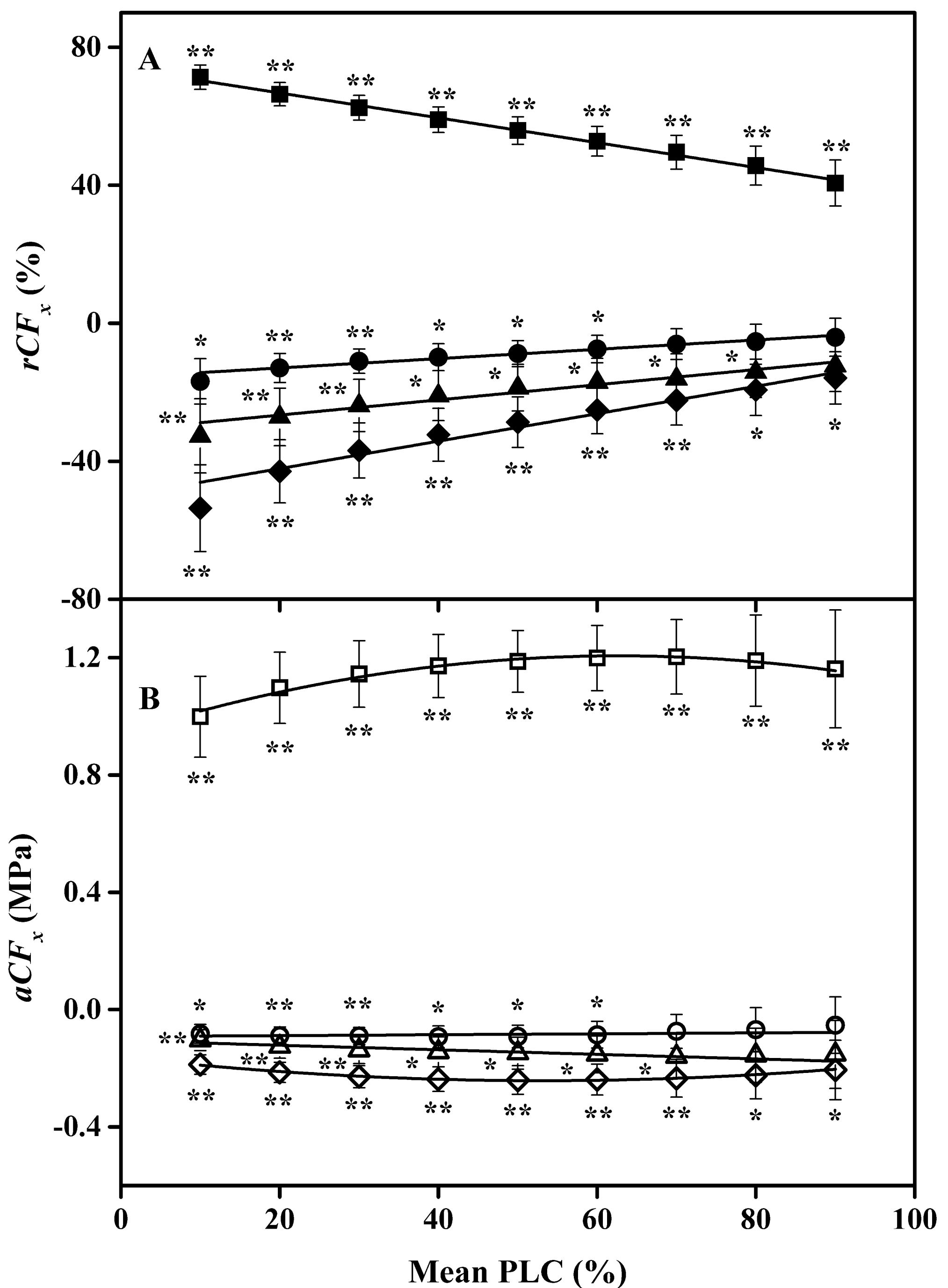


Figure 2. This shows two quantitative measures of cavitation-fatigue for KCl flushed samples. The fatigue values were calculated from the mean of the differences Eq. 3B (see methods), and is considered a more powerful test of differences between VCs. **A:** Mean relative cavitation-fatigue (rCF_x) versus x = the PLC at which rCF_x was evaluated. Solid squares compare 1st to 2nd VC, $y = -0.3612x + 74.012$ ($R^2 = 0.9952$, $p = 2E-09$); solid triangles compare 2nd to 3rd VC, $y = 0.2335x - 31.992$ ($R^2 = 0.9444$, $p = 1E-05$); solid circles compare 3rd to 4th VC, $y = 0.1436x - 16.341$ ($R^2 = 0.95$, $p = 8E-06$); and solid diamonds compare 2nd to 4th VC, $y = 0.43x - 52.274$ ($R^2 = 0.9489$, $p = 9E-06$). **B:** Mean change in absolute cavitation-fatigue (aCF_x) versus x = the PLC at which aCF_x was evaluated. Hollow squares compare 1st to 2nd VC, $y = -7E-05x^2 + 0.0086x + 0.9352$ ($R^2 = 0.9758$, $p = 1E-5$), however, the individual points were not different from each other significantly ($p = 0.334$); hollow triangles compare 2nd to 3rd VC, $y = -0.0006x - 0.1146$ ($R^2 = 0.7535$, $p = 0.0024$); hollow circles compare 3rd to 4th VC, $y = 0.0004x - 0.099$ ($R^2 = 0.5669$, $p = 0.019$); and hollow diamonds compare 2nd to 4th VC, $y = 3E-05x^2 - 0.0029x - 0.1636$ ($R^2 = 0.9877$, $p = 2E-6$). Error bars are SE. Symbols marked without ‘*’ marks were not significantly different from zero. The p -values in the linear regressions give the probability that the slope is zero.

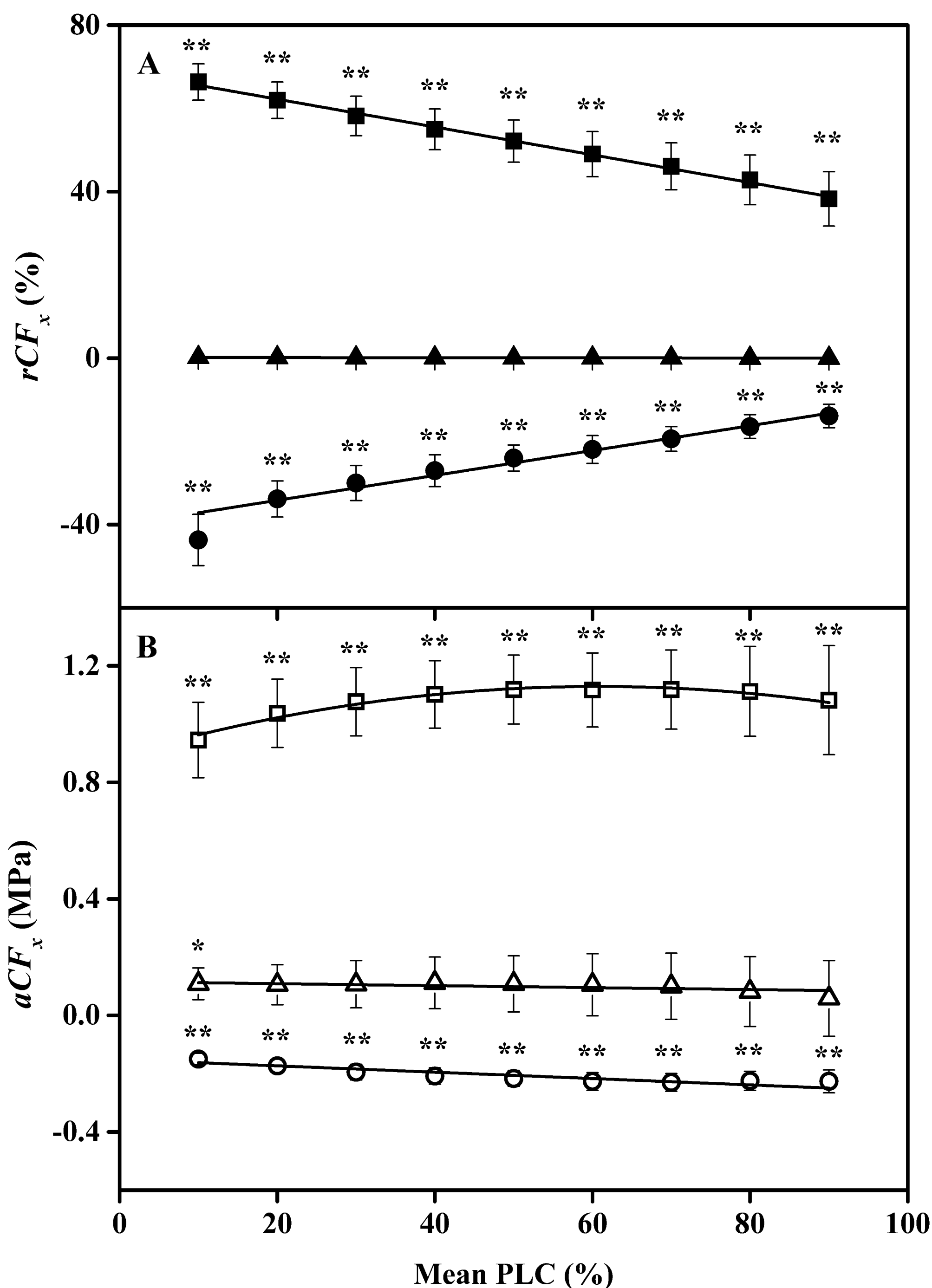


Figure 3. This shows two quantitative measures of cavitation-fatigue for CaCl_2 flushed samples. The fatigue values were calculated from the mean of the differences Eq. 3B (see methods), and is considered a more powerful test of differences between VCs. **A:** Mean relative cavitation-fatigue (rCF_x) versus $x =$ the PLC at which rCF_x was evaluated. Solid squares compare 1st to 2nd VC, $y = -0.3333x + 68.857$ ($R^2 = 0.9961$, $p = 1\text{E}-09$); solid triangles compare 2nd to 3rd VC, $y = -0.0018x + 0.1707$ ($R^2 = 0.9233$, $p = 4\text{E}-05$); and solid circles compare 3rd to 4th VC, $y = 0.3293x - 42.064$ ($R^2 = 0.9413$, $p = 1\text{E}-05$). **B:** Mean change in absolute cavitation-fatigue (aCF_x) versus $x =$ the PLC at which aCF_x was evaluated. Hollow squares compare 1st to 2nd VC, $y = -6\text{E}-05x^2 + 0.0078x + 0.8899$ ($R^2 = 0.9661$, $p = 4\text{E}-05$), however, the individuals were not different from each other significantly ($p = 0.408$); hollow triangles compare 2nd to 3rd VC, $y = -0.0005x + 0.1225$ ($R^2 = 0.58$, $p = 0.017$); hollow circles compare 3rd to 4th VC, $y = -0.0009x - 0.1599$ ($R^2 = 0.8087$, $p = 0.001$). Error bars are SE. Symbols with no ‘**’ marks were not significantly different from zero. The p -values in the linear regressions give the probability that the slope is zero.

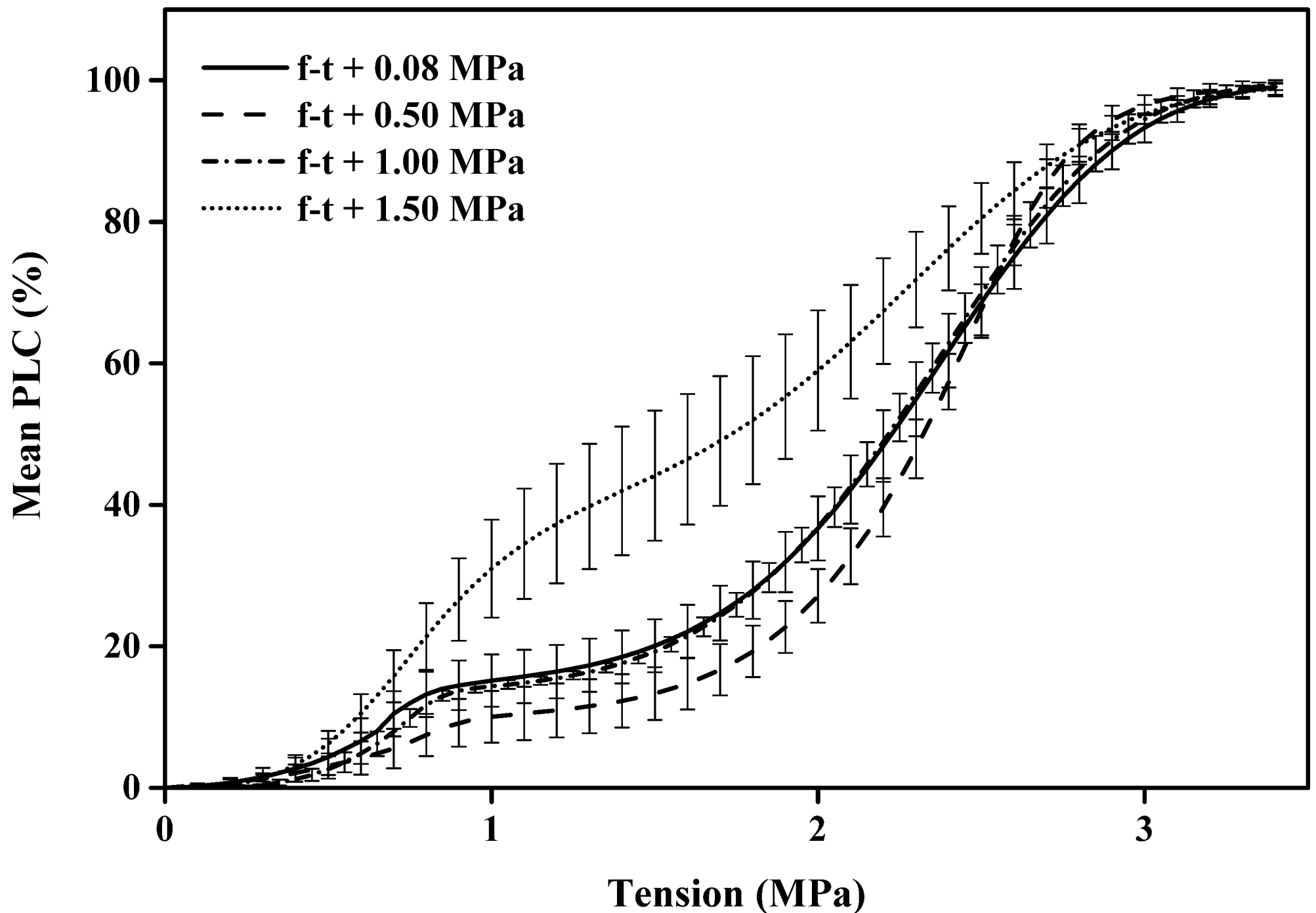


Figure 4. Vulnerability curves measured in stems following a freeze-thaw cycle (f-t) at varying tension. Frost induced embolism was removed by flushing before measuring the above VCs, hence the double s-curves were caused by frost-fatigue. The mean of 6~8 VCs were measured on flushed stems by the cavitron technique where each curve was fitted with a dual Weibull, then the mean and SE of all 6~8 best-fit curves were computed.

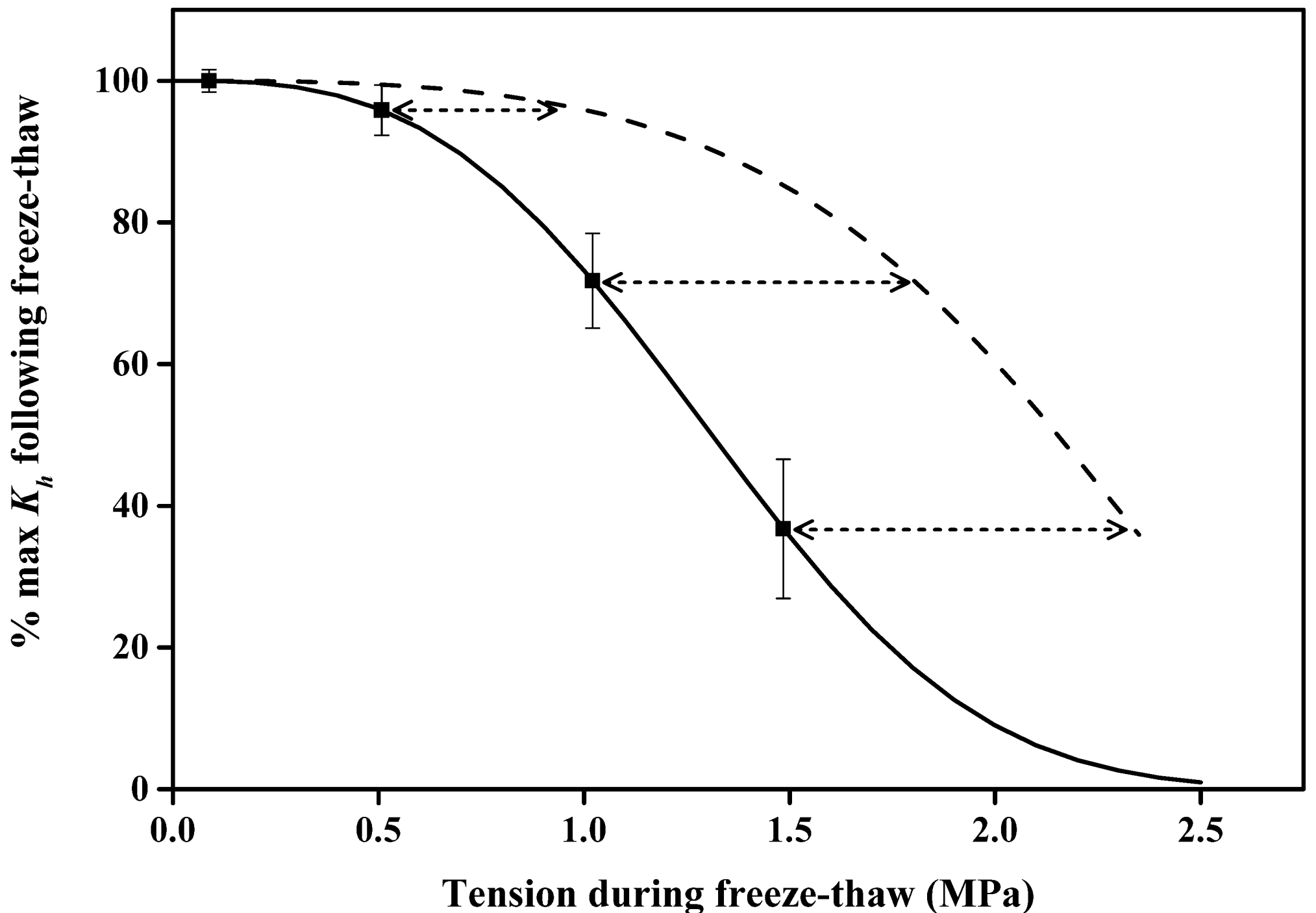


Figure 5. The squares show the impact of freezing on changes of K_h expressed as % of K_{max} before freezing. Error bars are \pm SE (N = 6 to 8). The y-axis can also be interpreted as 100% - the PLC induced by freezing + the tension on the x-axis. The solid line is a Weibull equation fit of the squares. The dashed line shows the mean impact of tension alone, without freezing, on % maximum K_h ; these values were re-plotted from the 1st VC in Fig. 1A (100% - PLC induced by tension alone). The double arrow can be interpreted as the amount of tension added by the freezing or thawing of tissue.

— Partial VC - - Full VC

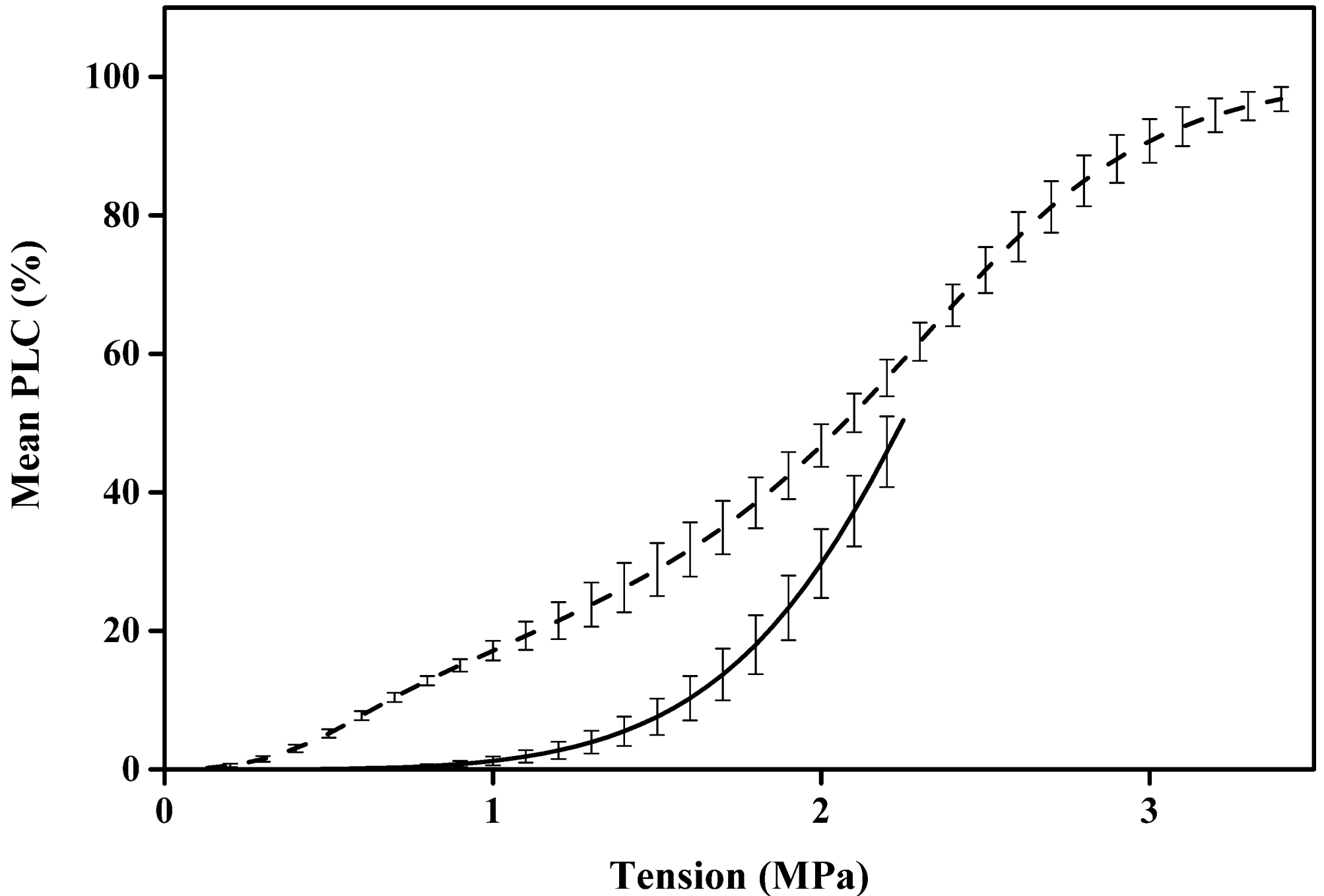


Figure 6. Vulnerability curves measured before and after 50 % embolism induced in stems. The mean and SE of all 6 best-fit curves before (solid curve) and after (dashed curve) 50 % embolism was induced by a tension of about 2.25 MPa; the stems were flushed between the first and second curve. The dashed curve was fitted with a dual Weibull, which is the sum of two s-shaped Weibull curves.

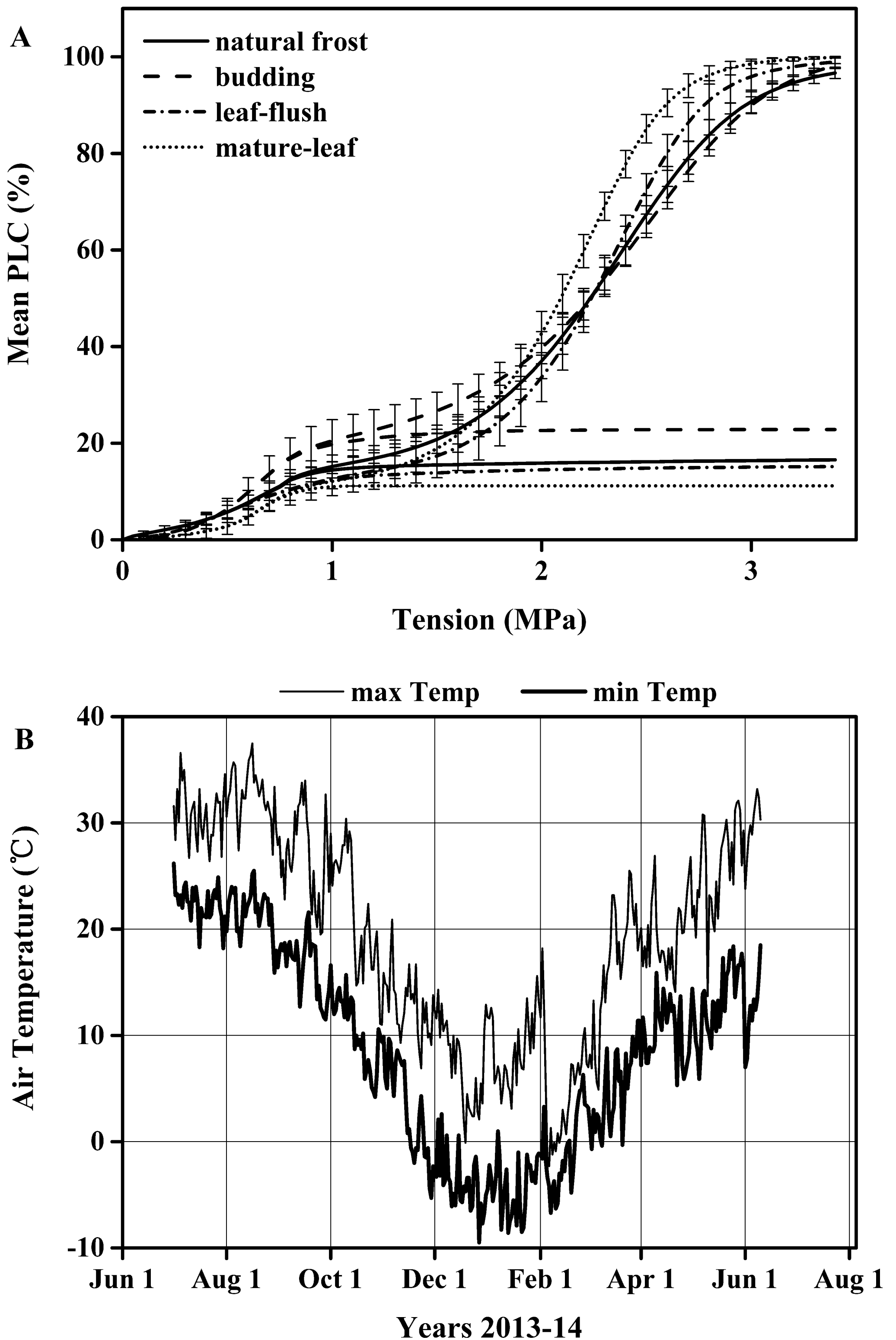


Figure 7. A: Vulnerability curves measured when stems were in four phenological phases, natural frost stage, budding stage, leaf-flush stage and mature-leaf stage. VCs measurements in the natural frost stage were based on N = 12 samples. VCs measurements in the budding stage and leaf-flush stage were based on N = 6 samples respectively. The mature-leaf stage were based on N = 7 samples. The mean of these VCs measured on flushed stems by the cavitrion technique where each curve was fitted with a dual Weibull, then the mean and SE were computed from the individual Weibull curves. The dual Weibull fit is the sum of two Weibull curves, the first s-shaped Weibull of each phonological phases are plotted to their theoretical plateaus for clarity and the plateau values on the y-axis = α in Eq. 2B. B: Shows a plot of minimum and maximum air temperatures recorded with 4 km of the location of the sampled trees.

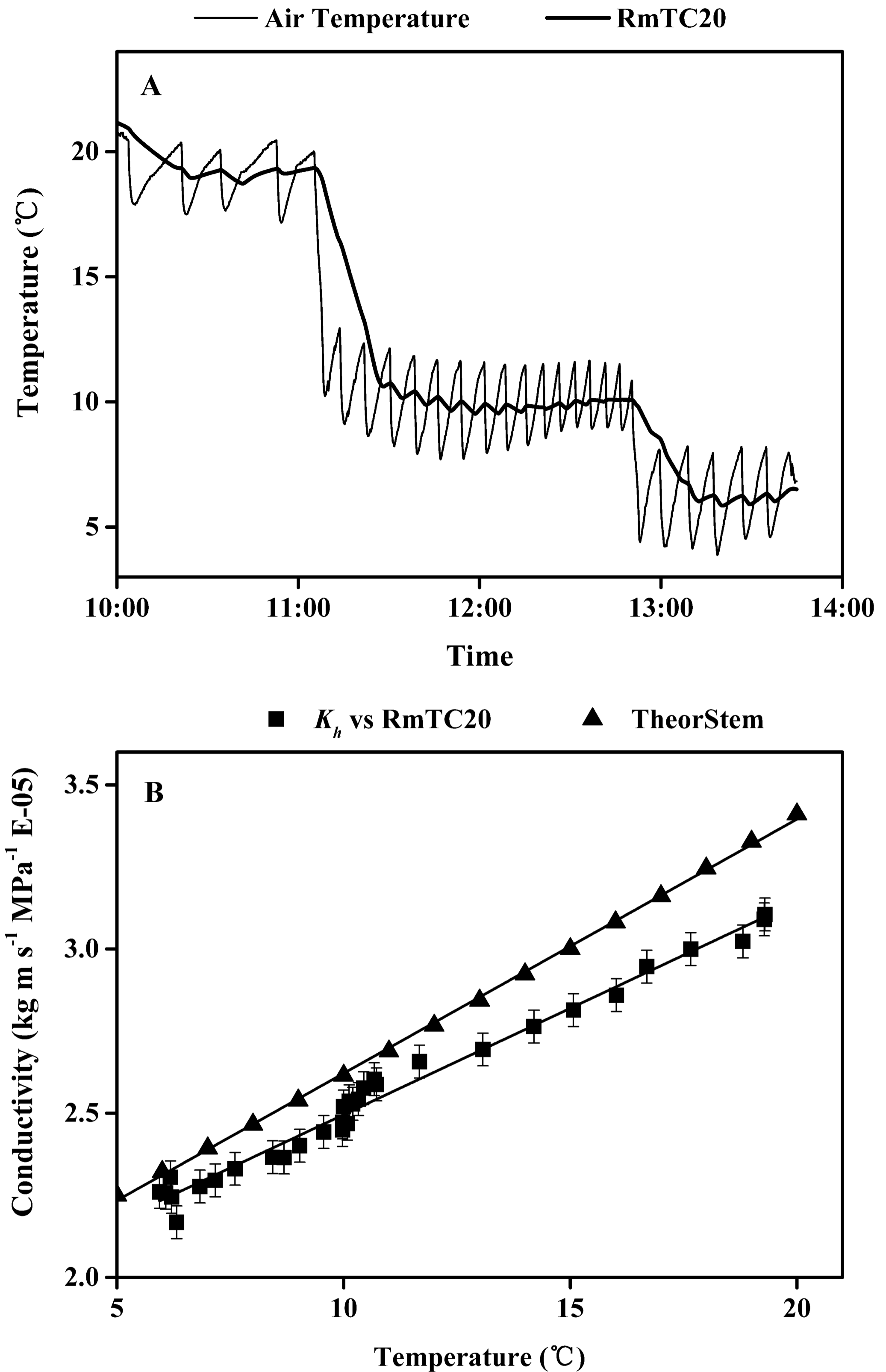


Figure 8. A: This shows the tempo of change in air temperature and the 20 min running mean of air temperature measured 2 cm from the rotor during the experiment shown in B. **B:** Shows the K_h in stem versus the 20 min running mean of air temperature (RmTC20). The regression of K_h versus RmTC20 was $y = 0.0648x + 1.8474$, $R^2 = 0.9826$, $p \leq 10^{-23}$, and the close correlation means that the 20 min running mean air temperature was an acceptable predictor of stem temperature. However the dependence of K_h on stem temperature was a less (lower slope) than predicted from 1/viscosity of water in an ideal pipe (TheorStem), which had a regression of $y = 0.0774x + 1.8472$, $R^2 = 0.9994$, $p \leq 10^{-23}$.

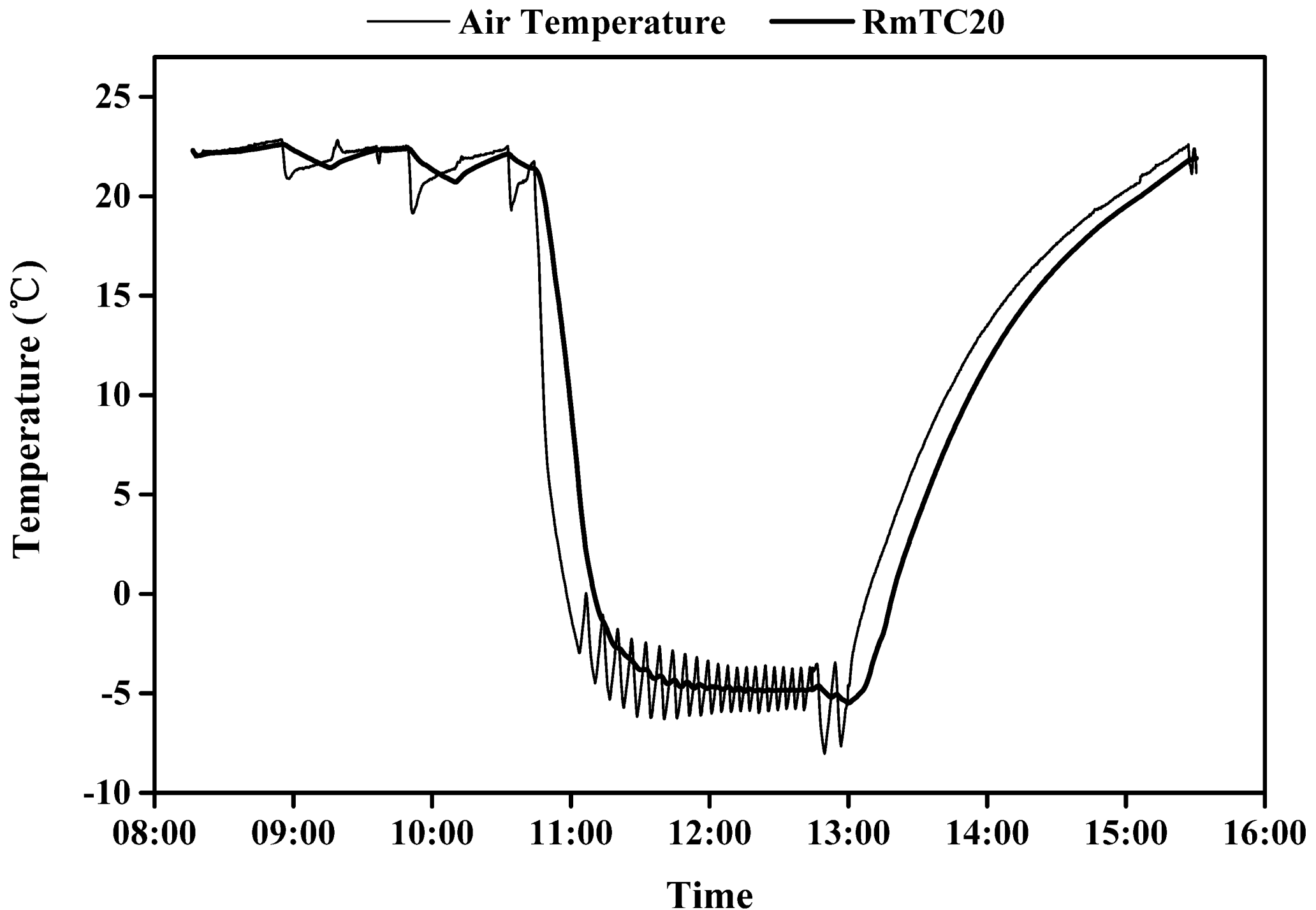


Figure 9. This shows a typical plot of temperature versus time for a typical freeze-thaw cycle. Air temperature (thin line) in the cavitrion was collected every 10s. However, 20 min running mean of air temperature (thick line) reflected more precisely the correct stem temperature (see Fig. 8). The stems thawed more slowly than they froze because the centrifuge did not have active heating; hence the stems and centrifuge was passively heated by the warm lab.